A Predictive Model of the Temperature-Dependent Inactivation of Coronaviruses

Te Faye Yap,[a] Zhen Liu,[a,†] Rachel A. Shveda,[a,†] Daniel J. Preston[a,*]

[a]Department of Mechanical Engineering, Rice University, 6100 Main St., Houston, TX 77006

[†]Denotes equal contribution

*To whom correspondence should be addressed: djp@rice.edu

ABSTRACT

The COVID-19 pandemic has stressed healthcare systems and supply lines, forcing medical doctors to risk infection by decontaminating and reusing medical personal protective equipment intended only for a single use. The uncertain future of the pandemic is compounded by limited data on the ability of the responsible virus, SARS-CoV-2, to survive across various climates, preventing epidemiologists from accurately modeling its spread. However, a detailed thermodynamic analysis of experimental data on the inactivation of SARS-CoV-2 and related coronaviruses can enable a fundamental understanding of their thermal degradation that will help mitigate the COVID-19 pandemic and future outbreaks. This paper introduces a thermodynamic model that synthesizes existing data into an analytical framework built on first principles, including the Arrhenius equation and the rate law, to accurately predict the temperature-dependent inactivation of coronaviruses. The model provides much-needed thermal sterilization guidelines for personal protective equipment, including masks, and will also allow epidemiologists to incorporate the lifetime of SARS-CoV-2 as a continuous function of environmental temperature into models forecasting the spread of coronaviruses across different climates and seasons.

INTRODUCTION

The COVID-19 pandemic has spread quickly and overwhelmed medical facilities worldwide, often resulting in a lack of intensive care beds and ventilators. These circumstances have forced doctors to decide which patients to provide with life-saving equipment—and which patients to leave without. The shortages have not only affected patients; facing a lack of masks, face shields, gowns, and other typically-disposable personal protective equipment (PPE), medical workers have had to reuse PPE or work without proper protection. As a result, many of them have been infected with SARS-CoV-2, the virus that causes COVID-19, despite the potential for effective sterilization techniques, including dry heat sterilization. Furthermore, as COVID-19 spreads to almost every region of the globe, epidemiologists need to know how long the virus survives in different climates in order to determine where to focus limited resources, how to model further spread, and how to predict future seasonal flare-ups.

During previous viral outbreaks, regional shortages of PPE led researchers to explore decontamination procedures that might allow PPE to be reused safely.[1,2] Facing an unprecedented nationwide lack of PPE brought on by the COVID-19 pandemic, medical workers have begun implementing these procedures: For example, The University of Nebraska Medical Center in Omaha began attempting in March 2020 to reuse masks after decontamination with ultraviolet (UV) irradiation.[3] However, UV decontamination faces several drawbacks, including an inability to kill viruses trapped within crevices that are not illuminated and a lack of availability in clinics in low-income areas and in most peoples' homes.[4] Other methods of decontamination, namely steam sterilization, alcohol washing, and bleach washing, are useful for items like glassware and other durable materials, but have been reported to degrade surgical masks and other delicate PPE not intended for reuse.[2,5,6] Dry heat sterilization, on the other hand, can be performed almost anywhere (including in home ovens intended for cooking), and viruses inside of crevices or within fabrics are easily inactivated. In addition, while dry heat sterilization is often performed at 160 °C or higher, it can effectively inactivate viruses at much lower temperatures as well (albeit over longer periods of time), enabling sterilization and reuse of delicate PPE intended for disposal after a

single use.[7] However, at this time, dry heat sterilization guidelines for single-use PPE contaminated with SARS-CoV-2 remain limited to only a few experimental measurements constrained to specific temperatures[8] and are not directly applicable to the temperatures encountered in home ovens and other heating devices. A predictive model that generates the necessary sterilization time at an arbitrary temperature would enable more robust guidelines applicable to any heating conditions.

Meanwhile, virus transmission has been linked to both seasonal and regional variations in climate, where colder atmospheric temperatures typically lead to longer virus lifetimes outside of their hosts. This effect has been reported for both influenza[9,10] and the common cold,[11] and even the human coronaviruses SARS-CoV-2,[8] SARS-CoV-1,[12,13] and MERS-CoV[14,15] have been shown to survive longer at lower temperatures. Unfortunately, existing data for SARS-CoV-2 is limited to specific experiments performed at only a few temperatures encountered in typical climates.[8,16] Epidemiologists would benefit from knowledge of the lifespan of SARS-CoV-2 as a continuous function of atmospheric temperature in order to accurately model the spread of COVID-19. Furthermore, understanding this temperature-dictated inactivation time could help predict whether the autumn and winter will bring a resurgence of cases as colder weather returns to the Northern Hemisphere, following a similar trend to that of the seasonal flu.[17]

In this work, we introduce an analytical model based on the rate law and Arrhenius equation that enables prediction of the thermal inactivation rate and lifetime of coronaviruses, including SARS-CoV-2, as a function of temperature. These viruses are treated as macromolecules undergoing thermal denaturation, and the time required to achieve a desired log-scale reduction in viable virions (e.g. by a factor of 10^6 as typically used for sterilization[18–21]) can be determined at a given temperature. We confirm that coronaviruses undergo thermal denaturation because their inactivation behavior follows the Meyer-Neldel rule.[22] Our model provides system-specific dry heat sterilization guidelines that may be used to safely decontaminate PPE at temperatures encountered in commonly-available equipment like home-use cooking ovens and rice cookers. The model also predicts the inactivation rate of human coronaviruses as a

continuous function of temperature in various climates; this ability will be of extreme importance to epidemiologists in predicting the regionally-dependent lifetime of the SARS-CoV-2 virus as well as the severity of the resurgence of COVID-19 that we may face this upcoming autumn and winter.

RESULTS

Reports in the literature describe the inactivation of many viruses over time, with experiments in different reports conducted over a range of temperatures, providing abundant data upon which a predictive analytical model capturing the influence of thermal effects on virus inactivation may be constructed. In this work, we focused specifically on the inactivation of coronaviruses, a group of enveloped viruses that contain positive sense single-stranded RNA and are often responsible for respiratory or gastrointestinal diseases in mammals and birds.[23] Specifically, we collected data on five types of coronaviruses, with subdivisions between types of viruses based on (i) strains of each virus, (ii) pH levels during experiments, and (iii) relative humidity conditions during experiments, resulting in fourteen sets of data (**Figure 1(a)**). These viruses include: (i) Severe Acute Respiratory Syndrome Coronavirus (both SARS CoV-1 and SARS-CoV-2);[8,13,16,24,25] (ii) Middle East Respiratory Syndrome Coronavirus (MERS-CoV);[14,15] (iii) Transmissible Gastroenteritis Virus (TGEV);[26] (iv) Mouse Hepatitis Virus (MHV);[27,28] and (v) Porcine Epidemic Diarrhea Virus (PEDV).[29] The first two types of viruses are highly pathogenic and cause life-threatening respiratory diseases in humans; SARS-CoV-2, the virus responsible for the COVID-19 pandemic, is closely related to SARS-CoV-1 and exhibits many chemical and biological similarities.[30] The latter three viruses are zoonotic viruses known to cause mild to severe illnesses in humans. In each of the referenced studies evaluating thermal inactivation characteristics of coronaviruses, viral inocula were exposed to different temperatures at varying time intervals. Samples were prepared by either suspending the viral stock in an appropriate test tube medium or depositing on a material surface. After exposure to different temperatures, samples on surfaces were recovered to a minimum essential medium. Either a plaque assay or a 50% tissue culture infectious dose ($TCID_{50}$) assay was used to evaluate the infectious titer; we converted $TCID_{50}$ results to number of plaque forming units (PFU) by multiplying by

0.69 based on theory, as performed in prior work.[31–33] Some of these reports also explored the effects of pH and relative humidity on viral infectivity.[26,29,34]

The inactivation behavior of microbes can be described accurately by the rate law.[35] Non-first-order rate laws have been applied to inactivation of some microbes,[36–38] particularly bacteria with heterogeneous populations,[39] but the inactivation of most viruses—including the viruses considered in our analysis—follows a first-order reaction, with viable virions as products and inactivated virions as reactants (Eq. 1):

$$[C] = [C_0]e^{-kt} \quad \text{(Eq. 1)}$$

The majority of primary experimental data for the inactivation of viruses is reported in plots of the log of concentration ln([C]) as a function of time. The rate constant, k, can be determined from the primary data by fitting a line to data taken at a given temperature, T, and calculating the slope, $k = \Delta\ln([C])/\Delta t$. Each of these pairs of (k, T) equate to one data point in **Figure 1(a)**. We fitted straight lines to the primary data for each of the viruses studied here in order to determine the rate constants of each virus corresponding to specific temperatures; these linear fits are included in the Supplementary Information.

Virus inactivation occurs due to thermal denaturation of the proteins that comprise each virion. The temperature dependence of this thermal denaturation process is captured by the Arrhenius equation,[40] which yields a linear relationship between ln(k) and 1/T (Eq. 2):

$$\ln(k) = -E_a/RT + \ln(A) \quad \text{(Eq. 2)}$$

where R is the gas constant, E_a is the activation energy associated with inactivation of the virus (i.e., the energy barrier that must be overcome for protein denaturation), and A is the frequency factor. Therefore, in **Figure 1(a)**, we applied linear fits to the data to enable continuous prediction of the reaction rates over the full range of temperatures. The activation energy, E_a, and natural log of the frequency factor, ln(A), were calculated for each virus by equating $-E_a/R$ and ln(A) from Eq. 2 with the slopes and intercepts from the linear fits in **Figure 1(a)**, respectively, according to the van't Hoff equation, and are plotted in **Figure 1(b)**. The correlation between ln(A) and E_a indicates that coronaviruses undergo a thermal denaturation

process following the Meyer-Neldel rule,[22] in support of our assertion that they are inactivated primarily by thermally-driven protein denaturation. In fact, the slope and intercept of a best-fit line applied to the data, for which we calculate [$\ln(A) = 0.394E_a - 5.63$] from the dataset used in this work, are nearly identical to the slopes and intercepts of [$\ln(A) = 0.380E_a - 5.27$][22] and [$\ln(A) = 0.383E_a - 5.95$][41] reported in prior work on denaturation of tissues and cells.

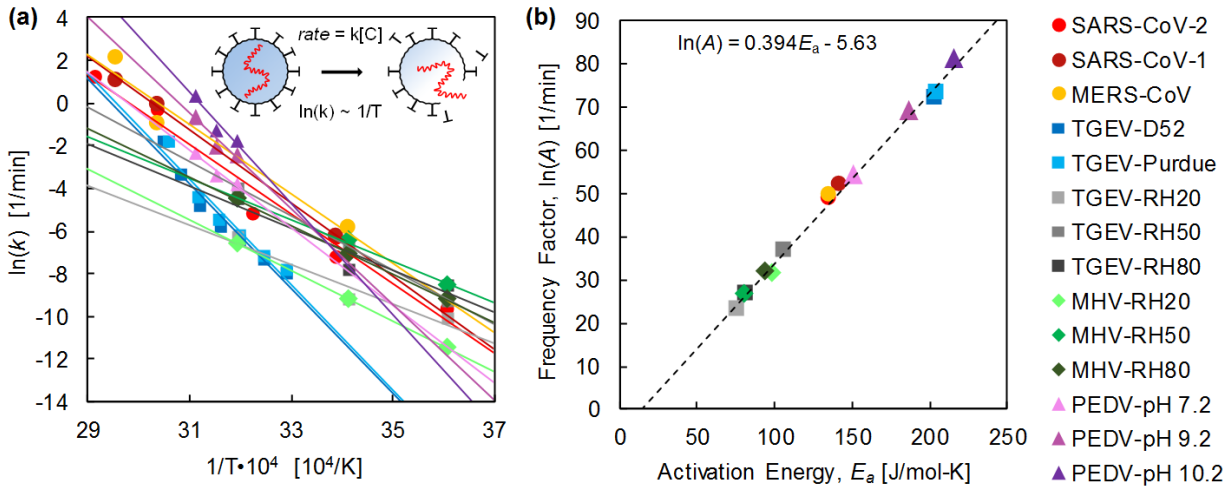

Figure 1. Thermal inactivation behavior of coronaviruses. *The dependence of inactivation rate on temperature was compiled from literature on several strains and under different relative humidity (RH) and pH conditions for SARS-CoV-2, SARS-CoV-1, MERS-CoV, TGEV, MHV, and PEDV, represented here in a van't Hoff plot (a). Each dataset was fitted with a linear curve according to Eq. 2, and the resulting activation energy and frequency factor were back-calculated from each linear fit according to Eq. 2 and plotted (b); the linear correlation between the log of frequency factor versus activation energy for the set of coronaviruses considered here supports our hypothesis that they are inactivated due to protein denaturation.*[22]

The degree of inactivation of a pathogen is defined by the ratio of the concentration (amount) of a pathogen compared to its initial concentration, [C]/[C_0], with varying levels of inactivation corresponding to rigor of sterilization reported in the literature, often in terms of orders of magnitude; an *n*-log

inactivation refers to a reduction in concentration of 10 raised to the *n*th power ($[C]/[C_0] = 10^{-n}$). Equations 1 and 2 combine to yield the time required to achieve an *n*-log reduction in a pathogen (Eq. 3):

$$t_{n-log} = -\frac{1}{A} e^{\left(\frac{E_a}{RT}\right)} \ln(10^{-n}) \quad \text{(Eq. 3)}$$

The US Food and Drug Administration recommends a 6-log reduction in concentration of a pathogen (i.e. $[C]/[C_0] = 10^{-6}$) for sterilization.[18–21] According to this recommendation, we refer to the time required to achieve a 6-log reduction as the virus lifetime, indicating both sterilization time and viable lifetime outside of a host. A more conservative value for sterilization could be modeled by inserting a different *n*-log value into Eq. 3, which would change all of the resulting predictions by a simple multiplicative factor of n/6 (e.g. to achieve a 12-log reduction in a virus would require doubling all of the times predicted in this work). The predictions generated from Eq. 3 are plotted in **Figure 2** and detailed in **Tables 1** and **2**.

Figure 2 shows the predictions of virus lifetime as a function of temperature ranging from room temperature to temperatures achievable using common heating devices. In **Figure 2(a)**, all five types of coronaviruses (subdivided according to virus strain and the experimental conditions of relative humidity and pH, as applicable) are plotted to show the variation across different environmental conditions and types of coronavirus. The plot in **Figure 2(b)** shows the same data, with the exception of data sourced from Casanova, et al.,[12] due to possible experimental error in the primary data from that report (see Supplementary Information, Section S3). The same data from **Figure 2(b)** is replotted in **Figure 2(c)** with the lifetime axis scaled linearly to highlight the exponential dependence of lifetime on temperature. **Figure 2(d)** focuses solely on the three human coronaviruses included in this work: SARS-CoV-2, SARS-CoV-1, and MERS-CoV exhibit a similar trend in thermal degradation, in agreement with recent work that has shown the inactivation behavior of SARS-CoV-2 is similar to SARS-CoV-1.[16] However, we observed that SARS-CoV-2 has a slightly longer lifetime than both SARS-CoV-1 and MERS-CoV outside of a host, potentially contributing to its relatively high reproduction number, R_0.

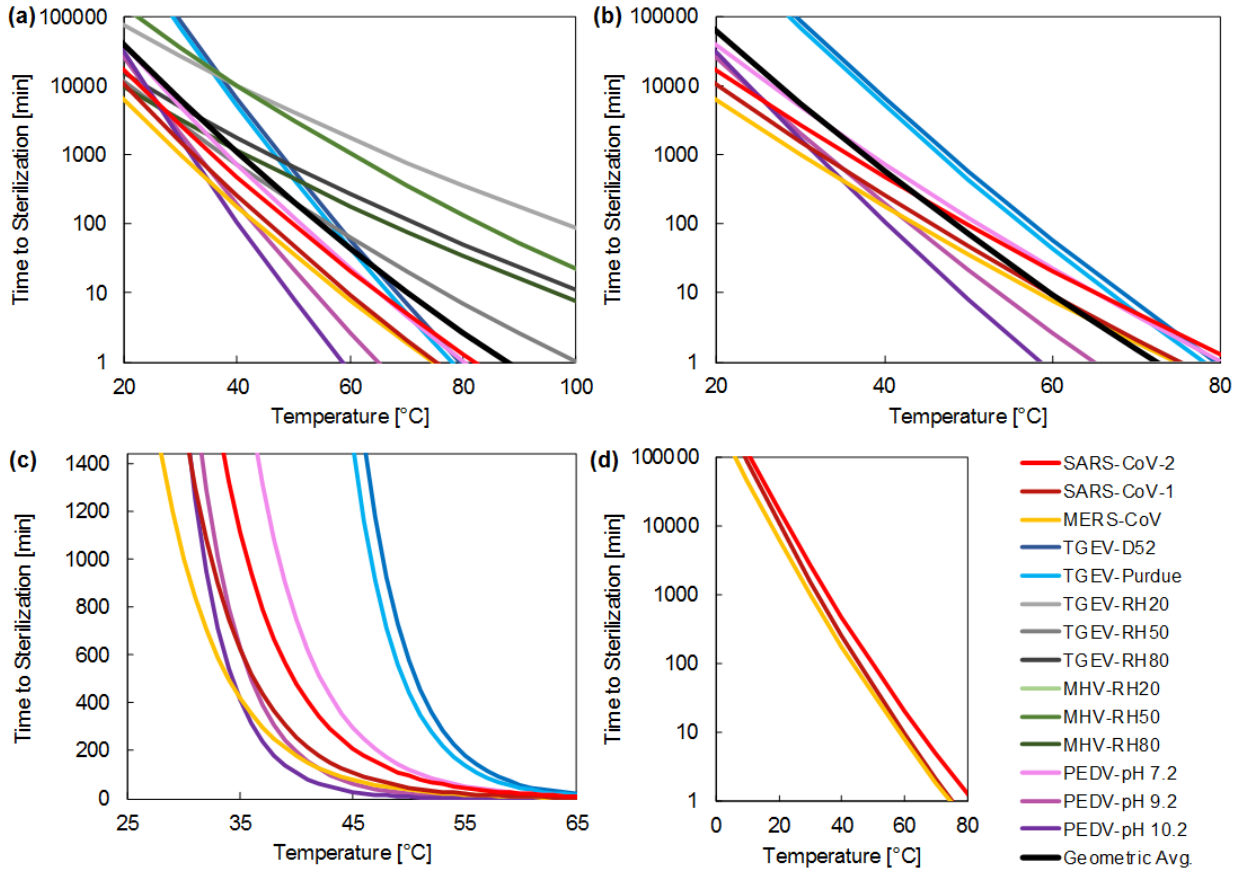

Figure 2. Virus lifetime as a function of temperature. *Predictions are shown for (a) all of the coronaviruses analyzed in this work and (b) all coronaviruses excluding the data from Casanova, et al., where the average curves apply to the data shown in each panel. The subset of data in (b) is replotted with a linearly-scaled vertical axis (1440 minutes = 1 day) to highlight the exponential dependence of sterilization time on temperature (c). The three human coronaviruses considered here have similar thermal degradation behavior and sterilization times (d), although SARS-CoV-2 exhibits a longer lifetime than both SARS-CoV-1 and MERS-CoV.*

The average sterilization times required for inactivation of all of the coronaviruses analyzed in this work, as well as the sterilization times for the subset of human coronaviruses (SARS-CoV-2, SARS-CoV-1, and MERS-CoV), are shown in **Table 1**. The temperature values displayed in the table were selected to illustrate that thermal sterilization is feasible at relatively low temperatures attainable by the general

public, albeit requiring longer sterilization times (most home ovens in the United States have a minimum temperature setting between 60-70 °C). The geometric mean was used to calculate the average coronavirus sterilization time for the full set of data, corresponding to the black curve in **Figure 2(a)**. The data shown in **Figure 2(d)** was used to tabulate the human coronavirus sterilization times, where sterilization of SARS-CoV-2 takes slightly longer than the other human coronaviruses but still less than the average time for all of the coronaviruses analyzed. Meanwhile, **Table 2** shows the lifetime of human coronaviruses outside of hosts, calculated based on thermal denaturation under different environmental temperatures, with the temperature range corresponding to seasonal weather patterns.

Table 1. *Sterilization time required for inactivation coronaviruses, with the average time for all of the coronaviruses analyzed in this work as well as for each of the human coronaviruses reported.*

Temperature	**Average coronavirus sterilization time, $t_{6\text{-log}}$**	**SARS-CoV-2 sterilization time, $t_{6\text{-log}}$**	**SARS-CoV-1 sterilization time, $t_{6\text{-log}}$**	**MERS-CoV sterilization time, $t_{6\text{-log}}$**
60 °C	45 min	21 min	9.5 min	7.9 min
70 °C	11 min	5.0 min	2.1 min	1.9 min
80 °C	2.7 min	1.3 min	< 1 min	< 1 min
90 °C	< 1 min	< 1 min	< 1 min	< 1 min

Table 2. *Lifetime of human coronaviruses outside of hosts across a range of environmental temperatures from 10 °C to 40 °C, defined as the time required for 6-log inactivation due to thermal denaturation (the lifetime of all human coronaviruses was greater than one month at temperatures below 10 °C).*

Temperature	**SARS-CoV-2 lifetime, $t_{6\text{-log}}$**	**SARS-CoV-1 lifetime, $t_{6\text{-log}}$**	**MERS-CoV lifetime, $t_{6\text{-log}}$**
10 °C	> 1 month	> 1 month	> 1 month
15 °C	30.0 d	20.8 d	11.5 d
20 °C	11.8 d	7.5 d	4.3 d
25 °C	4.6 d	2.8 h	1.7 d
30 °C	1.9 d	1.1 h	0.7 d
35 °C	18.7 h	10.4 h	7.0 h
40 °C	8.0 h	4.3 h	3.0 h

Depending on regional temperatures, coronavirus inactivation times may vary significantly. We estimated the lifetime of SARS-CoV-2 based on regional temperatures in the United States. We used temperatures averaged over January to March, 2020, corresponding to the onset of the COVID-19 pandemic (**Figure 3(a)**), and July to September, 2019, as a rough prediction of typical SARS-CoV-2 lifetimes in summer 2020 (**Figure 3(b)**). Virus lifetimes were determined using Eq. 3 and the appropriate E_a and ln(A) data (details in the Supplementary Information, Section S4). Summer weather in the Northern Hemisphere will reduce SARS-CoV-2 lifetime significantly as temperatures rise, potentially lowering the reproduction number, R_0, and slowing transmission of COVID-19. The predictions in **Figure 3** are based on a simplified constant temperature profile and do not account for daily temperature fluctuations, which may result in shorter lifetimes than predicted due to the exponential dependence of reaction rate on temperature. Additional environmental effects, like UV from sunlight, may further reduce inactivation time; with these limitations in mind, predicted thermal lifetimes longer than one month are not reported. The values shown in **Figure 3** represent maximum possible virus lifetimes across the United States.

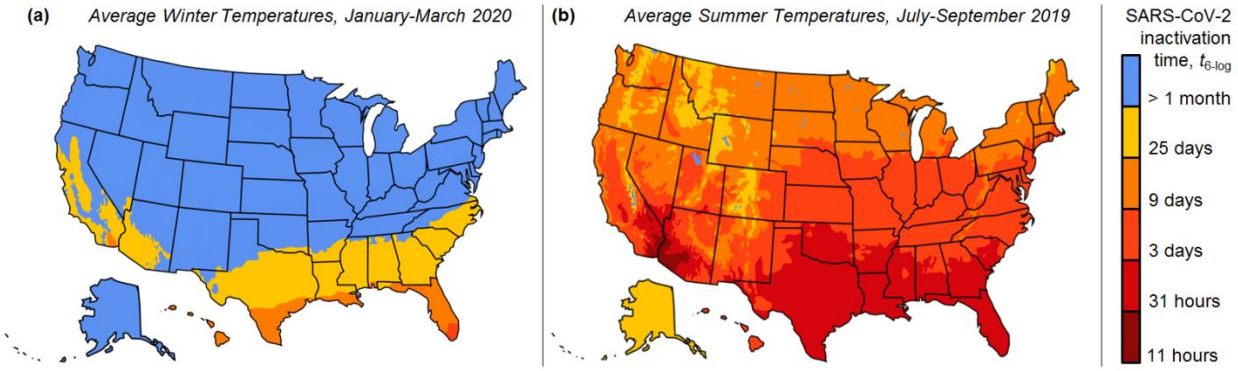

Figure 3. Lifetime of SARS-CoV-2 outside of a host across the United States in winter and summer. *Predictions are based on (a) average temperature data from January to March, 2020 (corresponding to the onset of COVID-19 pandemic), and (b) average temperature data from July to September, 2019 (to show characteristic lifetimes in summer weather). The lifetime of SARS-CoV-2 will decrease in summer, likely hindering transmission and lowering the reproduction number, R_0, but a recurrence of COVID-19 in autumn and winter may occur due to an increase in R_0 as the colder weather returns.*

DISCUSSION

We compared results from the thermodynamic model presented here with experimental data that had not been used as part of the model training data in order to test its predictive ability. SARS-CoV-1 has been reported to require 5 days at room temperature to achieve a 5-log reduction;[42] our model predicts am inactivation time of 4.2 days under the same conditions, in good agreement with the reported data. In another report, SARS-CoV-1 was heated to 56 °C and required only 6 minutes to achieve a 6-log reduction;[25] our model predicts a time of 17 minutes. A third report claimed that SARS-CoV-1 required 30 minutes to achieve an approximately 6-log reduction at 60 °C; [43] our model predicts a time of 10 minutes. Considering the demonstrated similarity in inactivation behavior of SARS-CoV-1 and SARS-CoV-2,[16] as well as the similarity in our model predictions for different strains of other coronaviruses (**Figure S23**), the model presented here offers promise as a useful tool to estimate the thermally-dependent inactivation behavior of SARS-CoV-2.

This model is limited to temperature-based predictive ability, and does not incorporate other environmental variables like the relative humidity and the fomite (i.e. the surface material on which a virion rests), both of which appear to have an effect on inactivation times.[8,12,16,44] Variations in inactivation time at a given temperature due to these environmental factors may be interpreted as catalytic effects,[45] where the activation energy is lowered on certain fomites, in the presence of water vapor, or even under different pH levels as observed in this work for PEDV (effect shown in **Figure S26**). Incorporating such an adjustment to the activation energy into the present model would enable predictive capability for other environmental conditions in addition to temperature. Another limitation of this model is its reliance on a limited set of primary data taken under different conditions which may also contain experimental error (all primary data is reproduced in the Supplementary Information). This model also assumes that the enthalpy and entropy of the inactivation reaction are constant as temperature changes, which is typically valid for macromolecules like proteins,[22] but the extrapolation of our model to higher

243 temperatures outside the range of the primary data (e.g. above 100 °C) may be unfounded if new
244 inactivation reaction pathways become available.
245
246 Fortunately, the results in **Table 1** indicate that dry heat sterilization is feasible for inactivation of all
247 types of coronaviruses, including SARS-CoV-2. The most common material used in surgical masks and
248 N95 respirators is non-woven polypropylene.[46,47] Polypropylene is mainly used in room temperature
249 conditions, already well above its glass transition temperature[48,49] and within a region of near-constant
250 stiffness until approaching its melting point, which is typically within the range of 156 °C to 168 °C.[50,51]
251 Cui and colleagues suggest that thermal cycling (75 °C, 30 min heating, applied over 20 cycles) does not
252 degrade the filtration efficiency of N95-level facial masks,[7] and Lin et al. have shown that there is no
253 significant degradation of surgical masks after heating to 160 °C for 3 min.[5] Therefore, we expect that
254 repeated sterilization at lower temperatures will be effective without degrading masks, while also feasible
255 within relatively short times (less than 30 min; **Table 1**) and achievable for the majority of humans with
256 access to home ovens, rice cookers, or similar inexpensive heating devices.
257
258 In summary, this work provides guidelines to medical professionals and the general public for the
259 effective, safe thermal sterilization of PPE, including surgical masks, gowns, and face shields, and even
260 the cloth masks—already popular worldwide—that the CDC has recommended all US citizens wear
261 during the COVID-19 pandemic.[52] In addition, the sensitivity of coronaviruses to environmental
262 temperature variations, shown in **Table 2** and **Figure 3**, indicates that the thermal inactivation of SARS-
263 CoV-2 must be considered in epidemiological studies predicting its global spread and, potentially,
264 seasonal recurrence; our model will be easily incorporated into these studies due to its ability to predict
265 virus lifetime as a continuous function of environmental temperature. Finally, the modeling framework
266 and predictions for the behavior of a wide range of coronaviruses presented here offers a new
267 fundamental understanding of their thermal inactivation that will help fight not only the COVID-19
268 pandemic but also future outbreaks of other novel coronaviruses.

METHODS

Data were obtained from the literature and homogenized according to the following procedures: (i) units were converted to standard SI, except for the use of minutes instead of seconds following the convention used in virology; (ii) 50% tissue culture infectious dose ($TCID_{50}$) assay results were converted to number of plaque forming units (PFU) by multiplying by 0.69 based on theory, as performed in prior work;[31–33] (iii) logarithms were all converted to base-*e* (the natural logarithm); and (iv) data for which the experimental error overlapped the lower detection limit (LDL) of the experimental technique were excluded because they would artificially skew the resulting curve fits towards lower rate constants (i.e. lower slopes). The specific procedures used to process each dataset are detailed in the Supporting Information, and the linear fits to the primary data used to determine the inactivation rate constants for each virus and at each temperature are shown in **Supplementary Figures S1-S28**. The slopes and intercepts of each of these fits are compiled in **Table S1** and **Figure S29**, and the activation energies and frequency factors plotted in **Figure 1(b)** are reported in **Table S2**.

DATA AVAILABILITY

The authors confirm that all relevant data are included in the paper and supplementary information files.

REFERENCES

(1) Heimbuch, B. K.; Wallace, W. H.; Kinney, K.; Lumley, A. E.; Wu, C. Y.; Woo, M. H.; Wander, J. D. A Pandemic Influenza Preparedness Study: Use of Energetic Methods to Decontaminate Filtering Facepiece Respirators Contaminated with H1N1 Aerosols and Droplets. *Am. J. Infect. Control* **2011**. https://doi.org/10.1016/j.ajic.2010.07.004.

(2) Viscusi, D. J.; King, W. P.; Shaffer, R. E. Effect of Decontamination on the Filtration Efficiency of Two Filtering Facepiece Respirator Models. *J. Int. Soc. Respir. Prot.* **2007**.

(3) Kolata, G. As Coronavirus Looms, Mask Shortage Gives Rise to Promising Approach. *The New York Times*. **2020**.

(4) Cramer, A.; Tian, E.; Yu, S. H.; Galanek, M.; Lamere, E.; Li, J.; Gupta, R.; Short, M. P. Disposable N95 Masks Pass Qualitative Fit-Test But Have Decreased Filtration Efficiency after Cobalt-60 Gamma Irradiation. *medRxiv* **2020**. https://doi.org/10.1101/2020.03.28.20043471.

(5) Lin, T. H.; Tang, F. C.; Hung, P. C.; Hua, Z. C.; Lai, C. Y. Relative Survival of Bacillus Subtilis Spores Loaded on Filtering Facepiece Respirators after Five Decontamination Methods. *Indoor Air* **2018**. https://doi.org/10.1111/ina.12475.

(6) Viscusi, D. J.; Bergman, M. S.; Eimer, B. C.; Shaffer, R. E. Evaluation of Five Decontamination Methods for Filtering Facepiece Respirators. *Ann. Occup. Hyg.* **2009**. https://doi.org/10.1093/annhyg/mep070.

(7) Liao, D. L.; Xiao, W.; Yu, X.; Wang, H.; Zhao, D. M.; Wang, D. Q. Can N95 Facial Masks Be Used after Disinfection? And for How Many Times? *Rep. from Collab. Stanford Univ. 4C Air, Inc* **2020**.

(8) Chin, A. W. H.; Chu, J. T. S.; Perera, M. R. A.; Hui, K. P. Y.; Yen, H.-L.; Chan, M. C. W.; Peiris, M.; Poon, L. L. M. Stability of SARS-CoV-2 in Different Environmental Conditions. *The Lancet Microbe* **2020**. https://doi.org/10.1016/s2666-5247(20)30003-3.

(9) Lowen, A. C.; Steel, J. Roles of Humidity and Temperature in Shaping Influenza Seasonality. *J. Virol.* **2014**. https://doi.org/10.1128/jvi.03544-13.

(10) Petrova, V. N.; Russell, C. A. The Evolution of Seasonal Influenza Viruses. *Nature Reviews Microbiology*. **2018**. https://doi.org/10.1038/nrmicro.2017.118.

(11) Ikäheimo, T. M.; Jaakkola, K.; Jokelainen, J.; Saukkoriipi, A.; Roivainen, M.; Juvonen, R.; Vainio, O.; Jaakkola, J. J. K. A Decrease in Temperature and Humidity Precedes Human Rhinovirus Infections in a Cold Climate. *Viruses* **2016**. https://doi.org/10.3390/v8090244.

(12) Casanova, L. M.; Jeon, S.; Rutala, W. A.; Weber, D. J.; Sobsey, M. D. Effects of Air Temperature and Relative Humidity on Coronavirus Survival on Surfaces. *Appl. Environ. Microbiol.* **2010**. https://doi.org/10.1128/AEM.02291-09.

(13) Rabenau, H. F.; Cinatl, J.; Morgenstern, B.; Bauer, G.; Preiser, W.; Doerr, H. W. Stability and

Inactivation of SARS Coronavirus. *Med. Microbiol. Immunol.* **2005**. https://doi.org/10.1007/s00430-004-0219-0.

(14) van Doremalen, N.; Bushmaker, T.; Munster, V. J. Stability of Middle East Respiratory Syndrome Coronavirus (MERS-CoV) under Different Environmental Conditions. *Eurosurveillance* **2013**, *18* (38), 1–4. https://doi.org/10.2807/1560-7917.ES2013.18.38.20590.

(15) Leclercq, I.; Batéjat, C.; Burguière, A. M.; Manuguerra, J. C. Heat Inactivation of the Middle East Respiratory Syndrome Coronavirus. *Influenza Other Respi. Viruses* **2014**. https://doi.org/10.1111/irv.12261.

(16) van Doremalen, N.; Bushmaker, T.; Morris, D. H.; Holbrook, M. G.; Gamble, A.; Williamson, B. N.; Tamin, A.; Harcourt, J. L.; Thornburg, N. J.; Gerber, S. I.; Lloyd-Smith, J. O.; de Wit, E.; Munster, V. J. Aerosol and Surface Stability of SARS-CoV-2 as Compared with SARS-CoV-1. *N. Engl. J. Med.* **2020**. https://doi.org/10.1056/nejmc2004973.

(17) Lin, J.; Kang, M.; Zhong, H.; Zhang, X.; Yang, F.; Ni, H.; Huang, P.; Hong, T.; Ke, C.; He, J. Influenza Seasonality and Predominant Subtypes of Influenza Virus in Guangdong, China, 2004-2012. *J. Thorac. Dis.* **2013**. https://doi.org/10.3978/j.issn.2072-1439.2013.08.09.

(18) Ellis, J. L.; Titone, J. C.; Tomasko, D. L.; Annabi, N.; Dehghani, F. Supercritical CO2 Sterilization of Ultra-High Molecular Weight Polyethylene. *J. Supercrit. Fluids* **2010**. https://doi.org/10.1016/j.supflu.2010.01.002.

(19) Andersen, H. K.; Fiehn, N. E.; Larsen, T. Effect of Steam Sterilization inside the Turbine Chambers of Dental Turbines. *Oral Surg. Oral Med. Oral Pathol. Oral Radiol. Endod.* **1999**. https://doi.org/10.1016/S1079-2104(99)70271-4.

(20) Mastanaiah, N.; Johnson, J. A.; Roy, S. Effect of Dielectric and Liquid on Plasma Sterilization Using Dielectric Barrier Discharge Plasma. *PLoS One* **2013**. https://doi.org/10.1371/journal.pone.0070840.

(21) Rutala, W. A.; Weber, D. J. Low-Temperature Sterilization Technologies: Do We Need to Redefine “Sterilization”? *Infect. Control Hosp. Epidemiol.* **1996**.

https://doi.org/10.2307/30141007.

(22) Qin, Z.; Balasubramanian, S. K.; Wolkers, W. F.; Pearce, J. A.; Bischof, J. C. Correlated Parameter Fit of Arrhenius Model for Thermal Denaturation of Proteins and Cells. *Ann. Biomed. Eng.* **2014**. https://doi.org/10.1007/s10439-014-1100-y.

(23) Masters, P. S. The Molecular Biology of Coronaviruses. *Advances in Virus Research*. **2006**. https://doi.org/10.1016/S0065-3527(06)66005-3.

(24) Darnell, M. E. R.; Taylor, D. R. Evaluation of Inactivation Methods for Severe Acute Respiratory Syndrome Coronavirus in Noncellular Blood Products. *Transfusion* **2006**. https://doi.org/10.1111/j.1537-2995.2006.00976.x.

(25) Kariwa, H.; Fujii, N.; Takashima, I. Inactivation of SARS Coronavirus by Means of Povidone-Iodine, Physical Conditions and Chemical Reagents. In *Dermatology*; **2006**. https://doi.org/10.1159/000089211.

(26) Laude, H. Thermal Inactivation Studies of a Coronavirus, Transmissible Gastroenteritis Virus. *J. Gen. Virol.* **1981**. https://doi.org/10.1099/0022-1317-56-2-235.

(27) Lelie, P. N.; Reesink, H. W.; Lucas, C. J. Inactivation of 12 Viruses by Heating Steps Applied during Manufacture of a Hepatitis B Vaccine. *J. Med. Virol.* **1987**. https://doi.org/10.1002/jmv.1890230313.

(28) Saknimit, M.; Inatsuki, I.; Sugiyama, Y.; Yagami, K. Virucidal Efficacy of Physico-Chemical Treatments against Coronaviruses and Parvoviruses of Laboratory Animals. *Jikken Dobutsu.* **1988**. https://doi.org/10.1538/expanim1978.37.3_341.

(29) Quist-Rybachuk, G. V.; Nauwynck, H. J.; Kalmar, I. D. Sensitivity of Porcine Epidemic Diarrhea Virus (PEDV) to PH and Heat Treatment in the Presence or Absence of Porcine Plasma. *Vet. Microbiol.* **2015**. https://doi.org/10.1016/j.vetmic.2015.10.010.

(30) Xu, J.; Zhao, S.; Teng, T.; Abdalla, A. E.; Zhu, W.; Xie, L.; Wang, Y.; Guo, X. Systematic Comparison of Two Animal-to-Human Transmitted Human Coronaviruses: SARS-CoV-2 and SARS-CoV. *Viruses* **2020**. https://doi.org/10.3390/v12020244.

(31) Possee, R. D. Baculovirus Expression Vectors — A Laboratory Manual. *Trends Biotechnol.* **1993**. https://doi.org/10.1016/0167-7799(93)90146-z.

(32) Neill, K. O.; Huang, N.; Unis, D.; Clem, R. J. Rapid Selection against Arbovirus-Induced Apoptosis during Infection of a Mosquito Vector. *Proc. Natl. Acad. Sci. U. S. A.* **2015**. https://doi.org/10.1073/pnas.1424469112.

(33) Li, S.; Zhao, H.; Yang, H.; Hou, W.; Cruz-Cosme, R.; Cao, R.; Chen, C.; Wang, W.; Xu, L.; Zhang, J.; Zhong, W.; Xia, N.; Tang, Q.; Cheng, T. Rapid Neutralization Testing System for Zika Virus Based on an Enzyme-Linked Immunospot Assay. *ACS Infect. Dis.* **2020**. https://doi.org/10.1021/acsinfecdis.9b00333.

(34) Hulst, M. M.; Heres, L.; Hakze-van der Honing, R. W.; Pelser, M.; Fox, M.; van der Poel, W. H. M. Study on Inactivation of Porcine Epidemic Diarrhoea Virus, Porcine Sapelovirus 1 and Adenovirus in the Production and Storage of Laboratory Spray-Dried Porcine Plasma. *J. Appl. Microbiol.* **2019**. https://doi.org/10.1111/jam.14235.

(35) C.R., S. Thermobacteriology in Food Processing (2nd Ed). *New York Acad. Press* **1973**.

(36) Xiong, R.; Xie, G.; Edmondson, A. E.; Sheard, M. A. A Mathematical Model for Bacterial Inactivation. *Int. J. Food Microbiol.* **1999**. https://doi.org/10.1016/S0168-1605(98)00172-X.

(37) CERF, O. A REVIEW Tailing of Survival Curves of Bacterial Spores. *J. Appl. Bacteriol.* **1977**. https://doi.org/10.1111/j.1365-2672.1977.tb00665.x.

(38) Casolari, A. Microbial Death. In *Physiological Models in Microbiology: Volume II*; **2018**. https://doi.org/10.1201/9781351075640.

(39) Van Boekel, M. A. J. S. On the Use of the Weibull Model to Describe Thermal Inactivation of Microbial Vegetative Cells. *Int. J. Food Microbiol.* **2002**. https://doi.org/10.1016/S0168-1605(01)00742-5.

(40) Price, W. C. Thermal Inactivation Rates of Four Plant Viruses. *Arch. Gesamte Virusforsch.* **1940**. https://doi.org/10.1007/BF01245548.

(41) Wright, N. T. On a Relationship between the Arrhenius Parameters from Thermal Damage

Studies. *J. Biomech. Eng.* **2003**. https://doi.org/10.1115/1.1553974.

(42) Lai, M. Y. Y.; Cheng, P. K. C.; Lim, W. W. L. Survival of Severe Acute Respiratory Syndrome Coronavirus. *Clin. Infect. Dis.* **2005**. https://doi.org/10.1086/433186.

(43) Yunoki, M.; Urayama, T.; Yamamoto, I.; Abe, S.; Ikuta, K. Heat Sensitivity of a SARS-Associated Coronavirus Introduced into Plasma Products. *Vox Sang.* **2004**. https://doi.org/10.1111/j.1423-0410.2004.00577.x.

(44) Chan, K. H.; Peiris, J. S. M.; Lam, S. Y.; Poon, L. L. M.; Yuen, K. Y.; Seto, W. H. The Effects of Temperature and Relative Humidity on the Viability of the SARS Coronavirus. *Adv. Virol.* **2011**. https://doi.org/10.1155/2011/734690.

(45) Roduner, E. Understanding Catalysis. *Chemical Society Reviews*. **2014**. https://doi.org/10.1039/c4cs00210e.

(46) Bałazy, A.; Toivola, M.; Adhikari, A.; Sivasubramani, S. K.; Reponen, T.; Grinshpun, S. A. Do N95 Respirators Provide 95% Protection Level against Airborne Viruses, and How Adequate Are Surgical Masks? *Am. J. Infect. Control* **2006**, *34* (2), 51–57. https://doi.org/10.1016/j.ajic.2005.08.018.

(47) Belkin, N. L. The Surgical Mask: Are New Tests Relevant for OR Practice? *AORN J.* **2009**, *89* (5), 883–891. https://doi.org/10.1016/j.aorn.2008.09.016.

(48) Passaglia, E.; Martin, G. M. Variation of Glass Temperature with Pressure in Polypropylene. *J. Res. Natl. Bur. Stand. Sect. A Phys. Chem.* **1964**, *68A* (3), 273. https://doi.org/10.6028/jres.068a.024.

(49) Bu, H.-S.; Cheng, S.; Wunderlich, B. Addendum to the Thermal Properties of Polypropylene. *Die Makromol. Chemie, Rapid Commun.* **1988**, *9* (2), 75–77. https://doi.org/10.1002/marc.1988.030090205.

(50) Tiganis, B. E.; Shanks, R. A.; Long, Y. Effects of Processing on the Microstructure, Melting Behavior, and Equilibrium Melting Temperature of Polypropylene. *J. Appl. Polym. Sci.* **1996**, *59* (4), 663–671.

(51) Duran, K.; Duran, D.; Oymak, G.; Kiliç, K.; Öncü, E.; Kara, M. Investigation of the Physical Properties of Meltblown Nonwovens for Air Filtration. *Tekst. ve Konfeksiyon* **2013**, *23* (2), 136–142.

(52) Michael D. Shear; Sheila Kaplan. A Debate Over Masks Uncovers Deep White House Divisions. *The New York Times*. **2002**.

ACKNOWLEDGEMENTS

We gratefully acknowledge helpful discussions with Dr. Dimithree Kahanda and financial support from Rice University.

AUTHOR CONTRIBUTIONS

T.F.Y. and D.J.P. compiled and analyzed the data and developed the analytical model. All authors contributed to interpretation of results and writing and editing the manuscript. D.J.P. guided the work.

COMPETING INTERESTS

The authors declare no competing financial interests.

SUPPLEMENTARY INFORMATION FOR:

A Predictive Model of the Temperature-Dependent Inactivation of Coronaviruses

Te Faye Yap,[a] Zhen Liu,[a,†] Rachel A. Shveda,[a,†] Daniel J. Preston[a,*]

[a]Department of Mechanical Engineering, Rice University, 6100 Main St., Houston, TX 77006

[†]Denotes equal contribution;

*To whom correspondence should be addressed: djp@rice.edu

Table of Contents

S1. Homogenization of Virus Inactivation Data

Data were obtained from the literature and homogenized according to the procedures described in the Methods section of the main text. The specific procedure for each dataset and supporting plots showing linear fits to data points are detailed in this section.

Data for SARS-CoV-2

A 50% tissue culture infectious dose ($TCID_{50}$) assay was reported in the work by Chin, et al.[8] We converted the $TCID_{50}$ results to number of plaque forming units (PFU) by multiplying by 0.69 based on theory, as performed in prior work,[31–33] and then converted the data from $\log_{10}$ to the natural log before plotting against time and taking a linear fit. Linear fits for the data at 4 °C, 22 °C, 37 °C, 56 °C, and 70 °C

are presented in **Figures S1** through **S5**. The resulting slopes were used to determine the rate constants at these temperatures, reported in **Table S1**.

We followed the same procedure to homogenize data reported by van Doremalen, et al.,[16] for SARS-CoV-2 on a fomite of plastic, chosen over other fomites reported in the study because plastic is inert and has a minimal catalytic effect on changing the activation energy. The authors specify experimental conditions with a temperature between 21-23 °C; we used an intermediate value of 22 °C in this work. Data near the lower detection limit (LDL) were excluded from the analysis to avoid under-predicting the rate. A linear fit is presented in **Figure S6**. The resulting slopes were used to determine the rate constants at these temperatures, reported in **Table S1**.

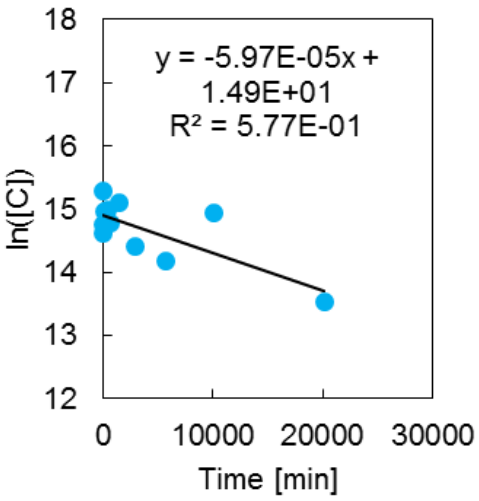

Figure S1. Primary data from Chin, et al.,[8] for inactivation of SARS-CoV-2 at 4 °C after converting the y-values from $TCID_{50}$ to PFU and from log_{10} to the natural log. We fit a line to the data to determine the rate constant at 4 °C.

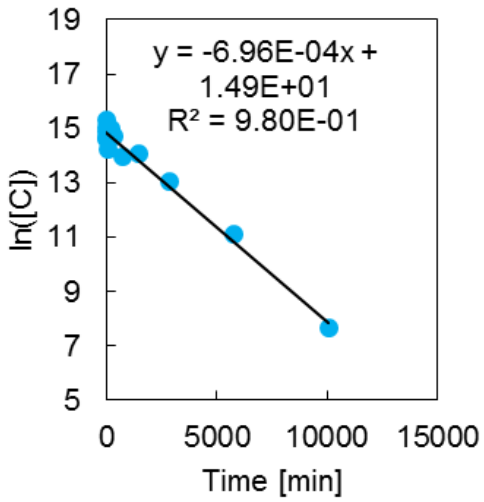

41

42 **Figure S2.** Primary data from Chin, et al.,[8] for inactivation of SARS-CoV-2 at 22 °C after converting the

43 y-values from $TCID_{50}$ to PFU and from log_{10} to the natural log. We fit a line to the data to determine the

44 rate constant at 22 °C.

45

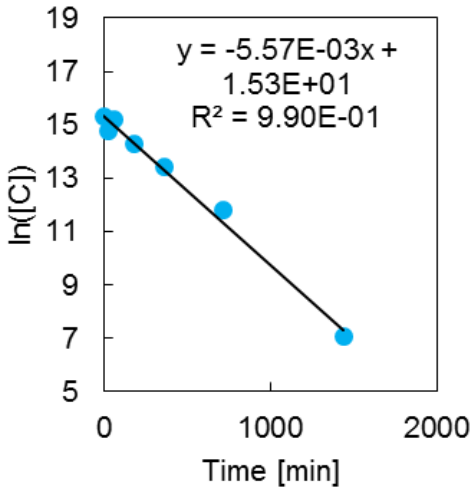

46

47 **Figure S3.** Primary data from Chin, et al.,[8] for inactivation of SARS-CoV-2 at 37 °C after converting the

48 y-values from $TCID_{50}$ to PFU and from log_{10} to the natural log. We fit a line to the data to determine the

49 rate constant at 37 °C.

50

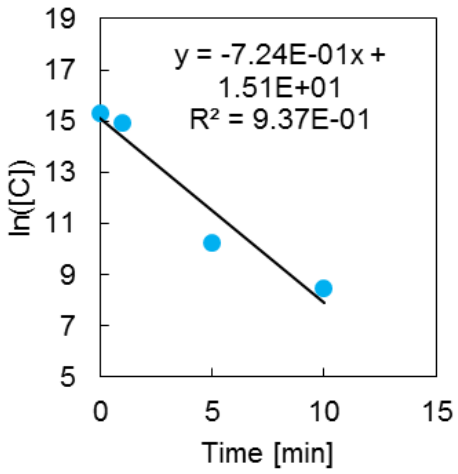

Figure S4. Primary data from Chin, et al.,[8] for inactivation of SARS-CoV-2 at 56 °C after converting the y-values from $TCID_{50}$ to PFU and from log_{10} to the natural log. We fit a line to the data to determine the rate constant at 56 °C.

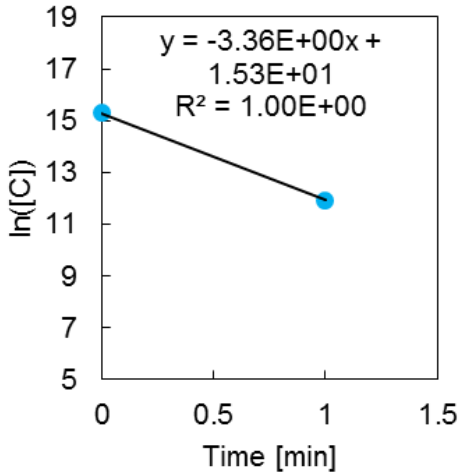

Figure S5. Primary data from Chin, et al.,[8] for inactivation of SARS-CoV-2 at 70 °C after converting the y-values from $TCID_{50}$ to PFU and from log_{10} to the natural log. We fit a line to the data to determine the rate constant at 70 °C.

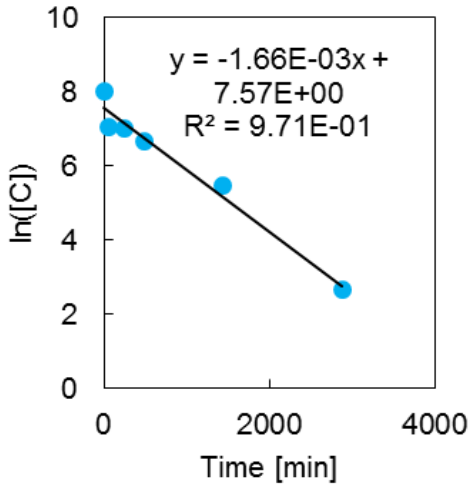

Figure S6. Primary data from van Doremalen, et al.,[16] for inactivation of SARS-CoV-2 at ≈22 °C after converting the y-values from $TCID_{50}$ to PFU and from $\log_{10}$ to the natural log. We fit a line to the data to determine the rate constant at 22 °C.

Data for SARS-CoV-1

A 50% tissue culture infectious dose ($TCID_{50}$) assay was reported in the work by Darnell, et al. We converted the $TCID_{50}$ results to number of plaque forming units (PFU) by multiplying by 0.69 based on theory, as performed in prior work,[31–33] and then converted the data from $\log_{10}$ to the natural log before plotting against time and taking a linear fit. Data near the lower detection limit (LDL) were excluded from the analysis to avoid under-predicting the rate. In addition, data at 75 °C were excluded because only one data point was not near the LDL, meaning a line could not be fit to the data. Linear fits for the data at 56 °C and 65 °C are presented in **Figures S7** and **S8**. The resulting slopes were used to determine the rate constants at these temperatures, reported in **Table S1**.

We followed the same procedure to homogenize data reported by van Doremalen, et al.,[16] for SARS-CoV-1 on a fomite of plastic, chosen over other fomites reported in the study because plastic is inert and has a minimal catalytic effect on changing the activation energy. The authors specify experimental

conditions with a temperature between 21-23 °C; we used an intermediate value of 22 °C in this work. Data near the lower detection limit (LDL) were excluded from the analysis to avoid under-predicting the rate. A linear fit is presented in **Figure S9**. The resulting slopes were used to determine the rate constants at these temperatures, reported in **Table S1**.

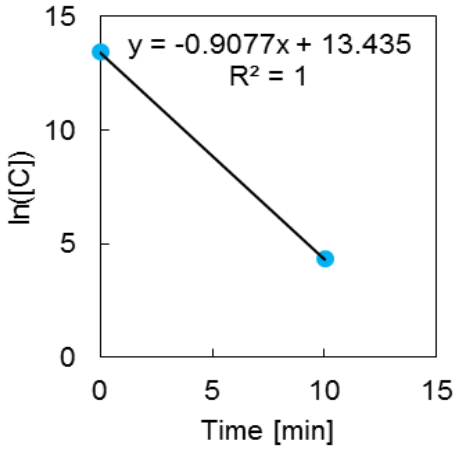

Figure S7. Primary data from Darnell, et al.,[24] for inactivation of SARS-CoV-1 at 56 °C after converting the y-values from $TCID_{50}$ to PFU and from log_{10} to the natural log. We fit a line to the data to determine the rate constant at 56 °C.

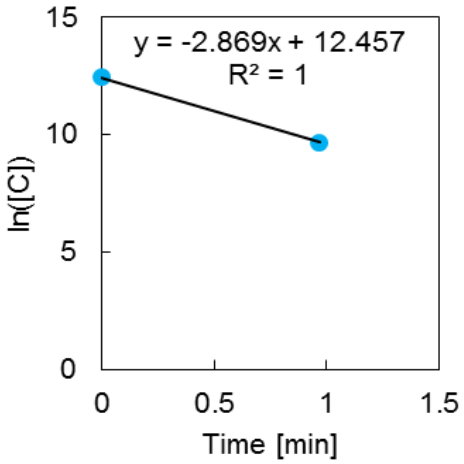

Figure S8. Primary data from Darnell, et al.,[24] for inactivation of SARS-CoV-1 at 65°C after converting the y-values from $TCID_{50}$ to PFU and from log_{10} to the natural log. We fit a line to the data to determine the rate constant at 65 °C.

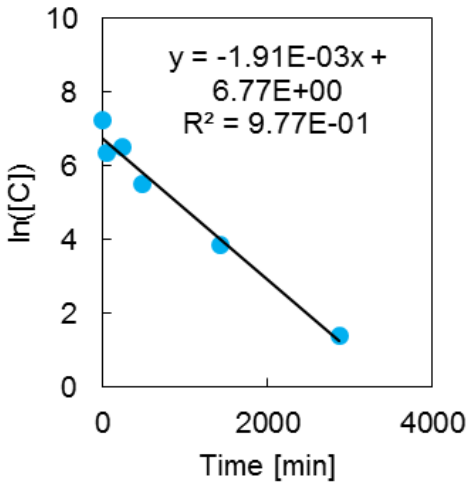

Figure S9. Primary data from van Doremalen, et al.,[16] for inactivation of SARS-CoV-1 at ≈22 °C after converting the y-values from $TCID_{50}$ to PFU and from $\log_{10}$ to the natural log. We fit a line to the data to determine the rate constant at 22 °C.

Data for MERS-CoV

A 50% tissue culture infectious dose ($TCID_{50}$) assay was reported in the work by Leclerq, et al. A table with information of the slopes (rate constant) at 56 °C and 65°C was provided. We converted the value of the slopes from $\log_{10}$ to the natural log and also the $TCID_{50}$ results to number of plaque forming units (PFU) by multiplying by 0.69 based on theory, as performed in prior work.[31–33] Data at 25°C were excluded due to the non-physical positive value for the slope (the concentration should decrease with time), which was likely due to experimental error in the measurements eclipsing the small change in concentration at 25°C. The authors also mentioned in the paper that there was no decrease in titre after 2 hours for the data taken at 25°C. The data for 20°C was obtained from work by Doremalen, et al. A $TCID_{50}$ assay was reported in their work. We converted $TCID_{50}$ results to number of plaque forming units (PFU) by multiplying by 0.69 based on theory, as performed in prior work,[31–33] and then converted the data from $\log_{10}$ to the natural log before plotting against time and taking a linear fit. A linear fit for the data at 20°C is presented in **Figure S10** and the slope is computed to determine the rate constant at this temperature, reported in **Table S1**.

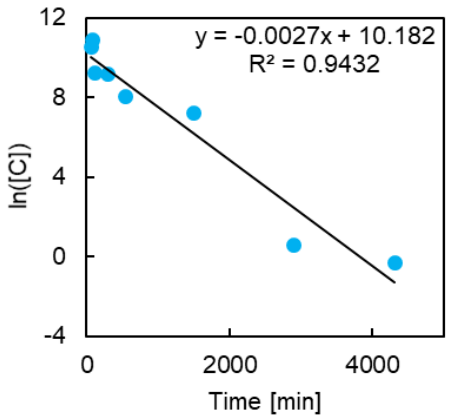

Figure S10. Primary data from van Doremalen, et al.,[14] for inactivation of MERS-CoV at 20 °C after converting the y-values from $TCID_{50}$ to PFU and from log_{10} to the natural log. We fit a line to the data to determine the rate constant at 20 °C.

Data for TGEV-D52 and TGEV-Purdue

An Arrhenius plot for thermal inactivation of TGEV D52 strain and Purdue strain was reported in the work by Laude, et al. The logarithms of the rate constants were provided for temperatures of 31, 35, 39, 43, 47, 51, and 55 °C. We converted the value of the rate constants from log_{10} to the natural log and also converted the units from inverse seconds to inverse minutes to maintain consistency with the other data values used in this work. The converted rate constants are reported in **Table S1**.

Data for TGEV at relative humidity (RH) values of 20%, 50%, and 80%

The virus concentration versus time for relative humidity (RH) values of 20%, 50%, and 80% at temperatures of 4, 20, and 40°C was reported in the work by Casanova, et al.[12] We converted the value of the slopes from log_{10} to the natural log before plotting against time and taking the linear fit to find the rate constant. Data near the lower detection limit (LDL) were excluded from the analysis to avoid under-predicting the rate (because the slope of the linear fit would artificially become shallower due to the inability to resolve lower concentrations experimentally). Linear fits for the data at 4, 20, and 40 °C and

at relative humidity values of 20%, 50%, and 80%, respectively, are shown in **Figures S11** to **S19**. The resulting slopes were used to determine the rate constants at these temperatures, reported in **Table S1**.

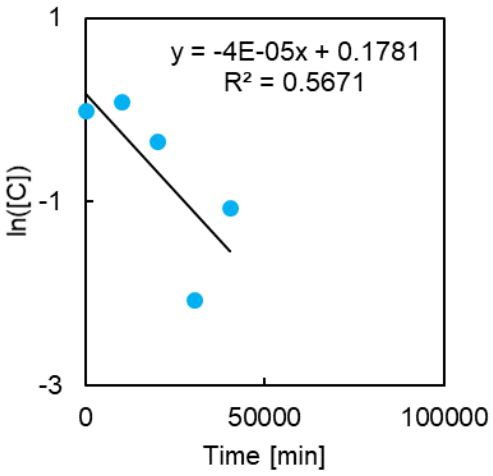

Figure S11. Primary data from Casanova et al.,[12] for inactivation of TGEV at 4 °C and relative humidity of 20% after converting the y-values from $\log_{10}$ to the natural log. We fit a line to the data to determine the rate constant at 4 °C and RH of 20%.

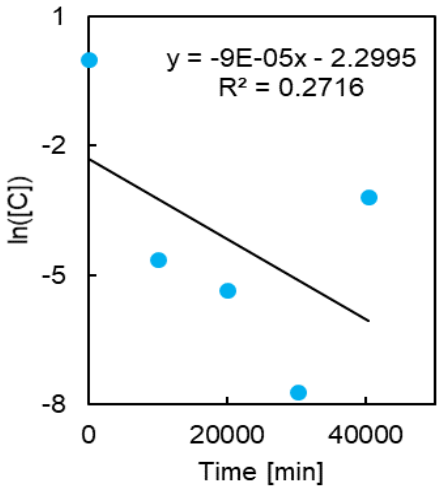

Figure S12. Primary data from Casanova et al.,[12] for inactivation of TGEV at 4 °C and relative humidity of 50% after converting values from $\log_{10}$ to the natural log. We fit a line to the data to determine the rate constant at 4 °C and RH of 50%.

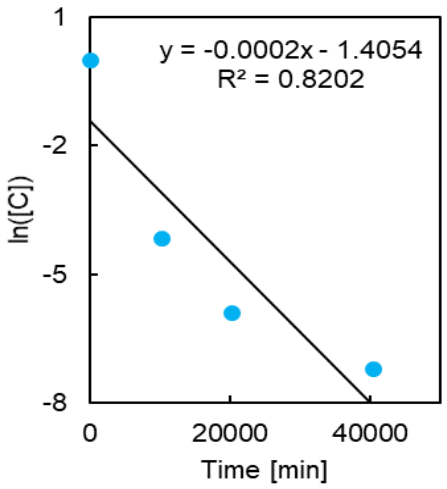

Figure S13. Primary data from Casanova et al.,[12] for inactivation of TGEV at 4 °C and relative humidity of 80% after converting values from $\log_{10}$ to the natural log. We fit a line to the data to determine the rate constant at 4 °C and RH of 80%.

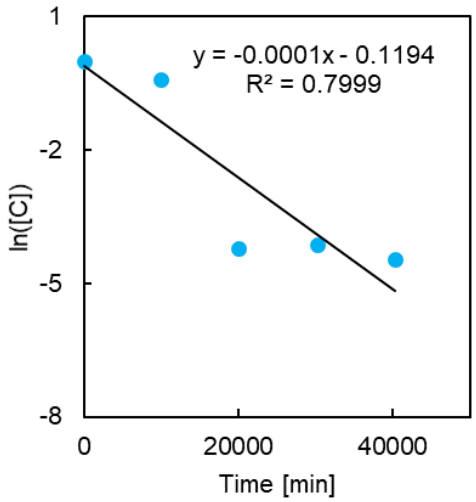

Figure S14. Primary data from Casanova et al.,[12] for inactivation of TGEV at 20 °C and relative humidity of 20% after converting values from $\log_{10}$ to the natural log. We fit a line to the data to determine the rate constant at 20 °C and RH of 20%.

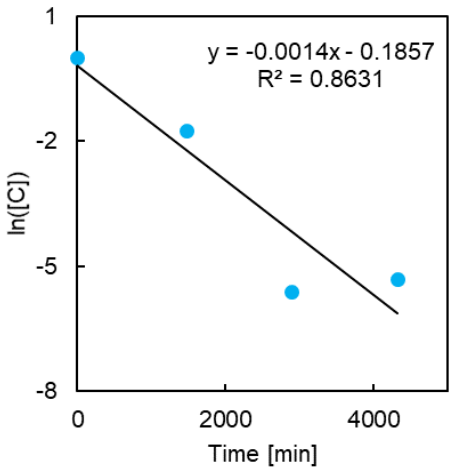

Figure S15. Primary data from Casanova et al.,[12] for inactivation of TGEV at 20 °C and relative humidity of 50% after converting values from $\log_{10}$ to the natural log. We fit a line to the data to determine the rate constant at 20 °C and RH of 50%.

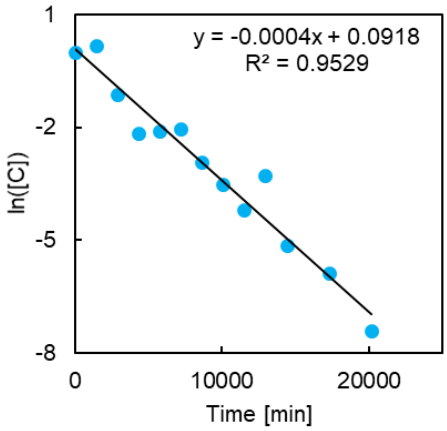

Figure S16. Primary data from Casanova et al.,[12] for inactivation of TGEV at 20 °C and relative humidity of 80% after converting values from $\log_{10}$ to the natural log. We fit a line to the data to determine the rate constant at 20 °C and RH of 80%.

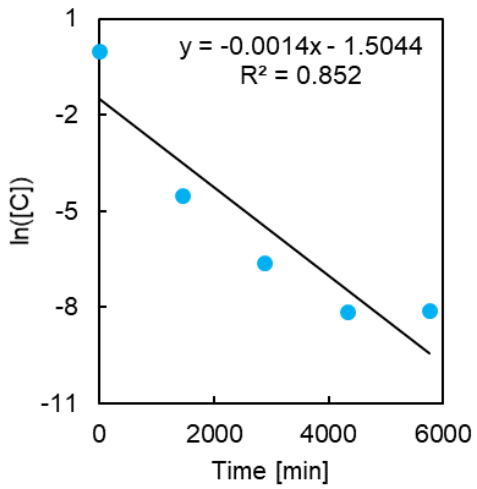

Figure S17. Primary data from Casanova et al.,[12] for inactivation of TGEV at 40 °C and relative humidity of 20% after converting values from $\log_{10}$ to the natural log. We fit a line to the data to determine the rate constant at 40 °C and RH of 20%.

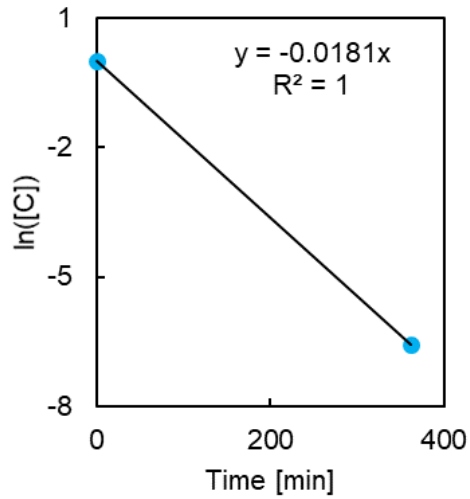

Figure S18. Primary data from Casanova et al.,[12] for inactivation of TGEV at 40 °C and relative humidity of 50% after converting values from $\log_{10}$ to the natural log. We fit a line to the data to determine the rate constant at 40 °C and RH of 50%.

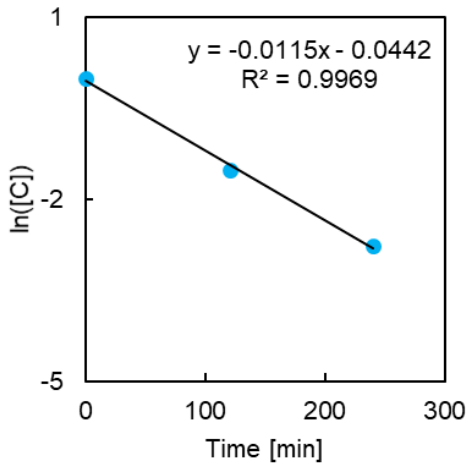

Figure S19. Primary data from Casanova et al.,[12] for inactivation of TGEV at 40 °C and relative humidity of 80% after converting values from $\log_{10}$ to the natural log. We fit a line to the data to determine the rate constant at 40 °C and RH of 80%.

Data for MHV at relative humidity (RH) values of 20%, 50%, and 80%

The virus concentration versus time for relative humidity (RH) values of 20%, 50%, and 80% at temperatures of 4, 20, and 40°C was reported in the work by Casanova, et al.[12] We converted the value of the slopes from $\log_{10}$ to the natural log before plotting against time and taking the linear fit to find the rate constant. Data near the lower detection limit (LDL) were excluded from the analysis to avoid under-predicting the rate (because the slope of the linear fit would artificially become shallower due to the inability to resolve lower concentrations experimentally). Linear fits for the data at 4, 20, and 40°C and at relative humidity values of 20%, 50%, and 80%, respectively, are shown in **Figures S20** to **S28**. The resulting slopes were used to determine the rate constants at these temperatures, reported in **Table S1**.

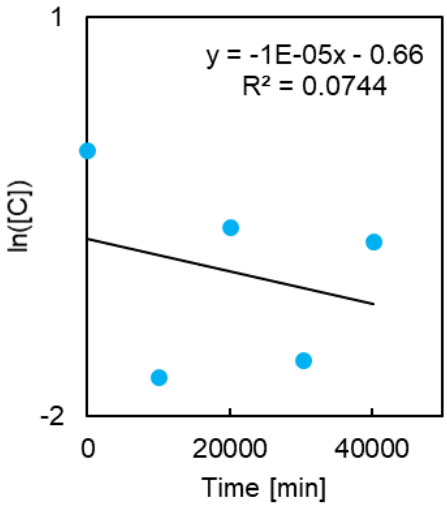

186

187 **Figure S20.** Primary data from Casanova et al.,[12] for inactivation of MHV at 4 °C and relative humidity
188 of 20% after converting values from $\log_{10}$ to the natural log. We fit a line to the data to determine the rate
189 constant at 4 °C and RH of 20%.

190

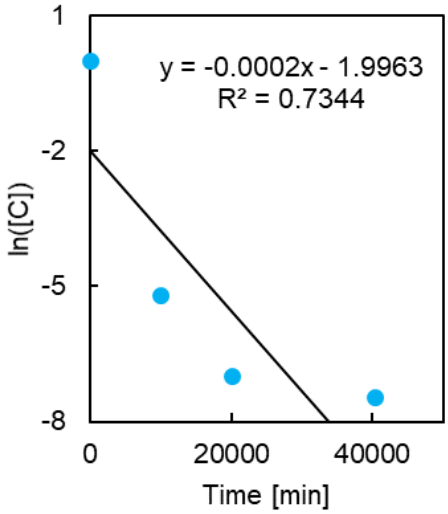

191

192 **Figure S21.** Primary data from Casanova et al.,[12] for inactivation of MHV at 4 °C and relative humidity
193 of 50% after converting values from $\log_{10}$ to the natural log. We fit a line to the data to determine the rate
194 constant at 4 °C and RH of 50%.

195

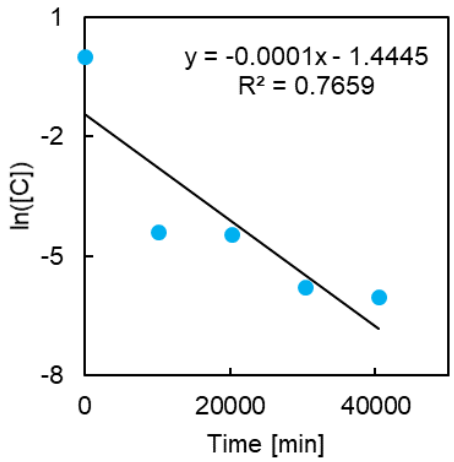

Figure S22. Primary data from Casanova et al.,[12] for inactivation of MHV at 4 °C and relative humidity of 80% after converting values from $\log_{10}$ to the natural log. We fit a line to the data to determine the rate constant at 4 °C and RH of 80%.

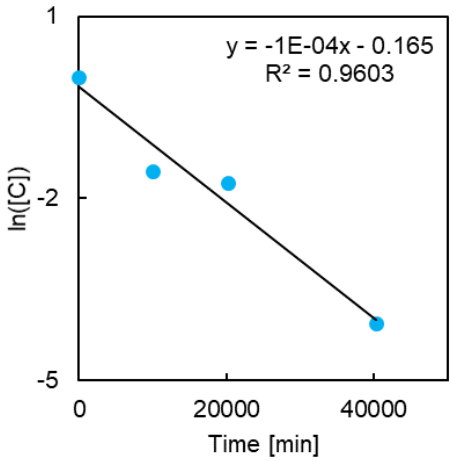

Figure S23. Primary data from Casanova et al.,[12] for inactivation of MHV at 20 °C and relative humidity of 20% after converting values from $\log_{10}$ to the natural log. We fit a line to the data to determine the rate constant at 20 °C and RH of 20%.

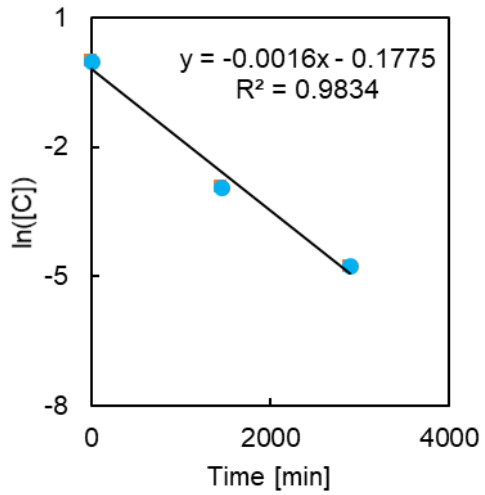

206

207 **Figure S24.** Primary data from Casanova et al.,[12] for inactivation of MHV at 20 °C and relative humidity
208 of 50% after converting values from $\log_{10}$ to the natural log. We fit a line to the data to determine the rate
209 constant at 20 °C and RH of 50%.

210

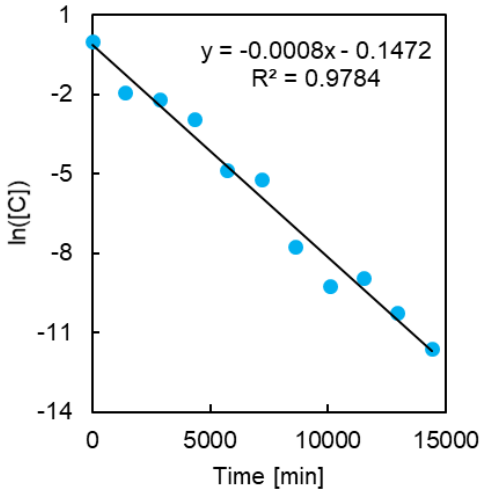

211

212 **Figure S25.** Primary data from Casanova et al.,[12] for inactivation of MHV at 20 °C and relative humidity
213 of 80% after converting values from $\log_{10}$ to the natural log. We fit a line to the data to determine the rate
214 constant at 20 °C and RH of 80%.

215

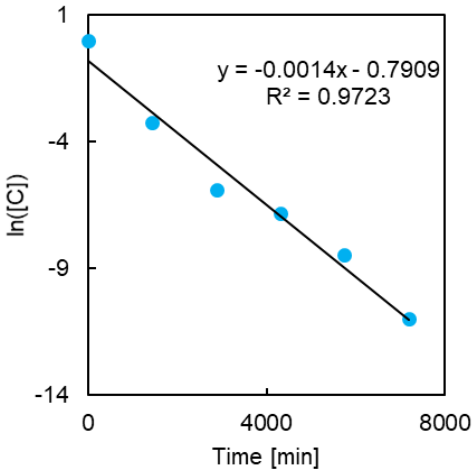

Figure S26. Primary data from Casanova et al.,[12] for inactivation of MHV at 40 °C and relative humidity of 20% after converting values from $\log_{10}$ to the natural log. We fit a line to the data to determine the rate constant at 40 °C and RH of 20%.

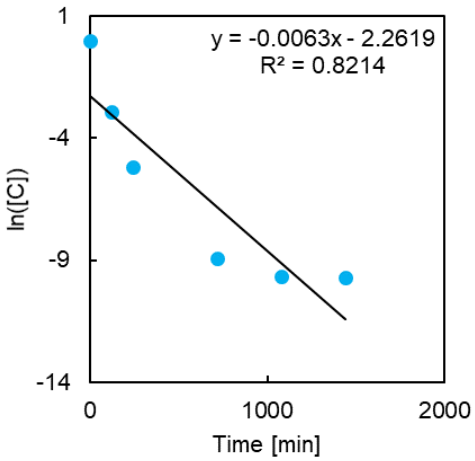

Figure S27. Primary data from Casanova et al.,[12] for inactivation of MHV at 40 °C and relative humidity of 50% after converting values from $\log_{10}$ to the natural log. We fit a line to the data to determine the rate constant at 40 °C and RH of 50%.

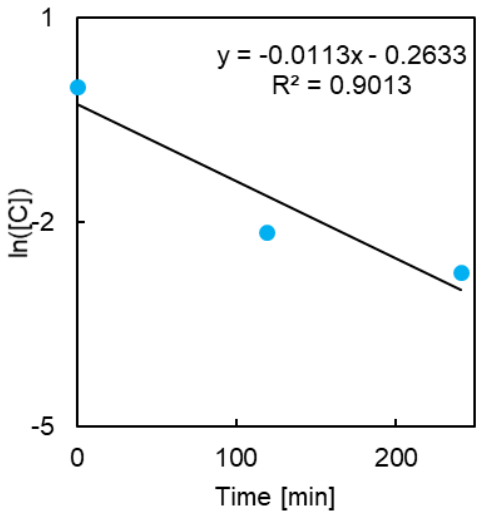

Figure S28. Primary data from Casanova et al.,[12] for inactivation of MHV at 40 °C and relative humidity of 80% after converting values from $\log_{10}$ to the natural log. We fit a line to the data to determine the rate constant at 40 °C and RH of 80%.

Data for PEDV at pH values of 7.2, 9.2, and 10.2

A 50% tissue culture infectious dose ($TCID_{50}$) assay was reported in the work by Quist-Rybachuk, et al. We converted $TCID_{50}$ results to number of plaque forming units (PFU) by multiplying by 0.69 based on theory, as performed in prior work,[31–33] and then converted the data from $\log_{10}$ to the natural log before calculating the slope based on the best fit lines that the authors provided in their plots. Data near the lower detection limit (LDL) had already been excluded from the authors' own analysis to avoid under-predicting the rate. The calculated slopes were used to determine the rate constants at 40, 44, and 48 °C for pH values of 7.2, 9.2, and 10.2, reported in **Table S1**.

S2. Processing of Virus Inactivation Data

This section contains all of the raw values for the processed data included in **Figure 1**. The data points in **Figure 1(a)** are listed in **Table S1**, where the ln(k) values were calculated from the $k = -\mathrm{d}(\ln([C]))/\mathrm{d}t$ values determined in **Section S1**, unless otherwise noted in the table. The slope-intercept data for all of the linear fits in **Figure 1** are listed in **Table S2** and shown in **Figure S29**, along with the calculated activation energy and frequency factor shown in **Figure 1(b)**.

Table S1. Data plotted in **Figure 1(a)** in the main text.

Dataset	Ref.	T [°C]	$1/T \cdot 10^4$ [10^4/K]	$k = -\mathrm{d}(\ln([C]))/\mathrm{d}t$ [1/min]	ln(k) [1/min]
SARS-CoV-2	[8]	4	36.10	0.0000597	-9.726
SARS-CoV-2	[8]	22	33.90	0.000696	-7.270
SARS-CoV-2	[16]	22	33.90	0.00166	-6.401
SARS-CoV-2	[8]	37	32.36	0.00557	-5.190
SARS-CoV-2	[8]	56	30.39	0.724	-0.323
SARS-CoV-2	[8]	70	29.15	3.36	1.212
SARS-CoV-1	[16]	22	33.90	0.00191	-6.261
SARS-CoV-1	[24]	56	30.40	0.9077	-0.097
SARS-CoV-1	[24]	65	29.59	2.869	1.054
MERS-CoV	[14]	20	34.13	0.0027	-5.914
MERS-CoV	[14]	56	30.40	0.16	-0.999
MERS-CoV	[14]	65	29.59	3.62	2.121
TGEV-D52	[26]	31	32.90	ln(k) provided in source	-7.963
TGEV-D52	[26]	35	32.47	ln(k) provided in source	-7.332
TGEV-D52	[26]	39	32.05	ln(k) provided in source	-6.439
TGEV-D52	[26]	43	31.65	ln(k) provided in source	-5.808
TGEV-D52	[26]	47	31.25	ln(k) provided in source	-4.837
TGEV-D52	[26]	51	30.86	ln(k) provided in source	-3.369
TGEV-D52	[26]	55	30.48	ln(k) provided in source	-1.823
TGEV-Purdue	[26]	31	32.90	ln(k) provided in source	-7.832

TGEV-Purdue	[26]	35	32.47	ln(*k*) provided in source	-7.149
TGEV-Purdue	[26]	39	32.05	ln(*k*) provided in source	-6.177
TGEV-Purdue	[26]	43	31.65	ln(*k*) provided in source	-5.468
TGEV-Purdue	[26]	47	31.25	ln(*k*) provided in source	-4.418
TGEV-Purdue	[26]	55	30.48	ln(*k*) provided in source	-1.849
TGEV-RH20	[12]	4	36.10	0.000042	-10.126
TGEV-RH20	[12]	20	34.13	0.00013	-9.210
TGEV-RH20	[12]	40	31.95	0.0014	-6.570
TGEV-RH50	[12]	4	36.10	0.000093	-9.316
TGEV-RH50	[12]	20	34.13	0.0014	-6.571
TGEV-RH50	[12]	40	31.95	0.0181	-4.012
TGEV-RH80	[12]	4	36.10	0.00017	-8.517
TGEV-RH80	[12]	20	34.13	0.00035	-7.824
TGEV-RH80	[12]	40	31.95	0.0115	-4.465
MHV-RH20	[12]	4	36.10	0.000012	-11.513
MHV-RH20	[12]	20	34.13	0.000095	-9.210
MHV-RH20	[12]	40	31.95	0.0018	-6.571
MHV-RH50	[12]	4	36.10	0.00017	-8.517
MHV-RH50	[12]	20	34.13	0.0016	-6.438
MHV-RH50	[12]	40	31.95	0.0114	-4.474
MHV-RH80	[12]	4	36.10	0.00013	-9.210
MHV-RH80	[12]	20	34.13	0.00080	-7.131
MHV-RH80	[12]	40	31.95	0.0113	-4.483
PEDV-pH 7.2	[29]	40	31.95	0.0211	-3.858
PEDV-pH 7.2	[29]	44	31.55	0.0326	-3.422
PEDV-pH 7.2	[29]	48	31.15	0.0900	-2.407
PEDV-pH 9.2	[29]	40	31.95	0.0863	-2.449
PEDV-pH 9.2	[29]	44	31.55	0.1295	-2.044
PEDV-pH 9.2	[29]	48	31.15	0.5178	-0.658
PEDV-pH 10.2	[29]	40	31.95	0.1618	-1.821
PEDV-pH 10.2	[29]	44	31.55	0.2728	-1.299
PEDV-pH 10.2	[29]	48	31.15	1.2943	0.258

248

Table S2. Slopes and intercepts of data plotted in **Figure 1(a)** in the main text, and the calculated ln(*A*) and E_a values shown in **Figure 1(b).**

Dataset	**Slope [K/10^4]**	**Intercept [1/min]**	**E_a [J/mol]**	**ln(*A*) [1/min]**
SARS-CoV-2	-1.632	48.617	135,692	48.62
SARS-CoV-1	-1.715	51.903	142,601	51.90
MERS-CoV	-1.628	49.480	135,377	49.48
TGEV-D52	-2.451	72.205	203,822	72.21
TGEV-Purdue	-2.472	73.094	205,509	73.09
TGEV-RH20	-0.924	22.919	76,826	22.92
TGEV-RH50	-1.276	36.811	106,051	36.81
TGEV-RH80	-0.986	26.640	81,964	26.64
MHV-RH20	-1.191	31.449	98,984	31.45
MHV-RH50	-0.972	26.644	80,850	26.64
MHV-RH80	-1.140	31.882	94,776	31.88
PEDV-pH7.2	-1.820	54.177	151,291	54.18
PEDV-pH9.2	-2.245	69.111	186,661	69.11
PEDV-pH10.2	-2.606	81.262	216,676	81.26

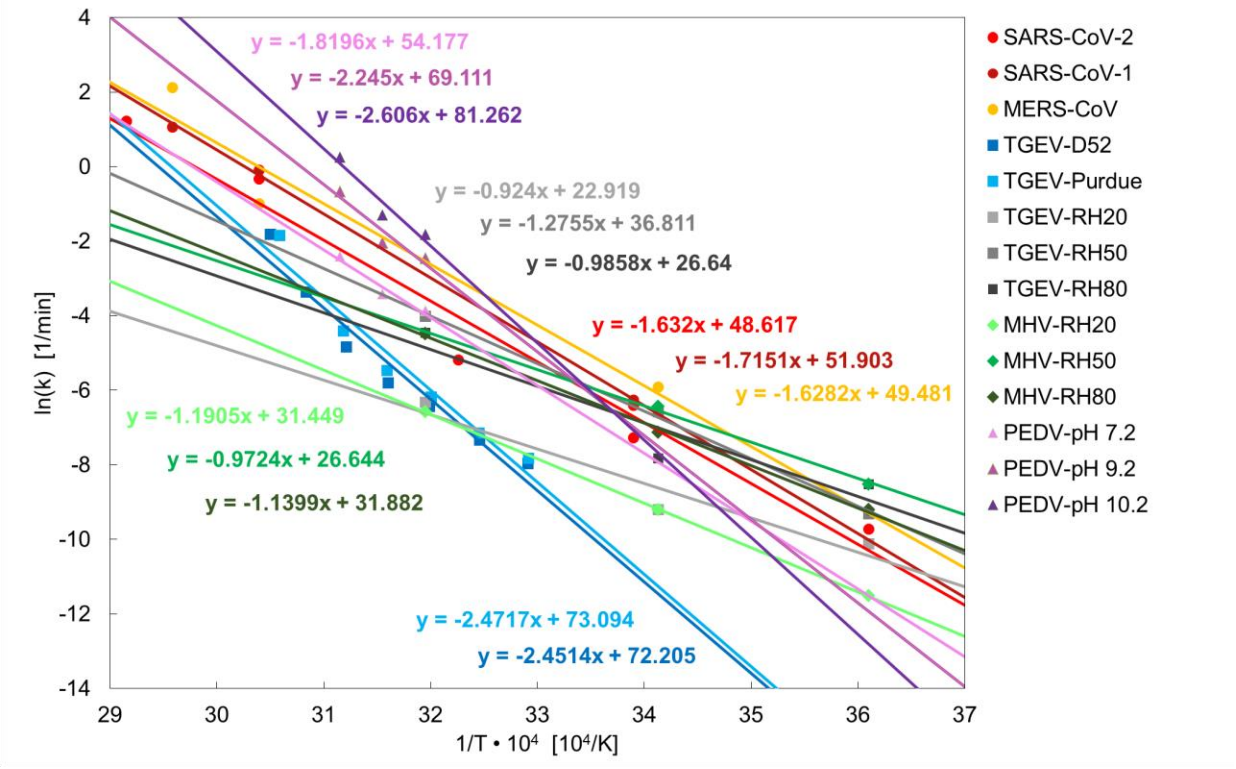

Figure S29. A magnified version of **Figure 1(a)** from the main text, with the slopes and intercepts for each linear fit indicated.

S3. Trends across Virus Strains, Relative Humidity, and pH

Subsets of the model predictions for several viruses that varied only by strain, relative humidity, or pH of the surrounding medium are plotted here to more clearly highlight trends.

Trends across virus strains

Comparing results for the TGEV-D52 and TGEV-Purdue strains, we did not observe any significant deviation in the model prediction between these strains, shown in **Figure S30.** We hypothesize that the similarity between these two strains may be indicative of a similarity that SARS-CoV-2 could exhibit with SARS-CoV-1; we have predictive capability for SARS-CoV-1 with the present model and data, and the predictions for SARS-CoV-1 may suggest the expected thermal degradation of SARS-CoV-2.

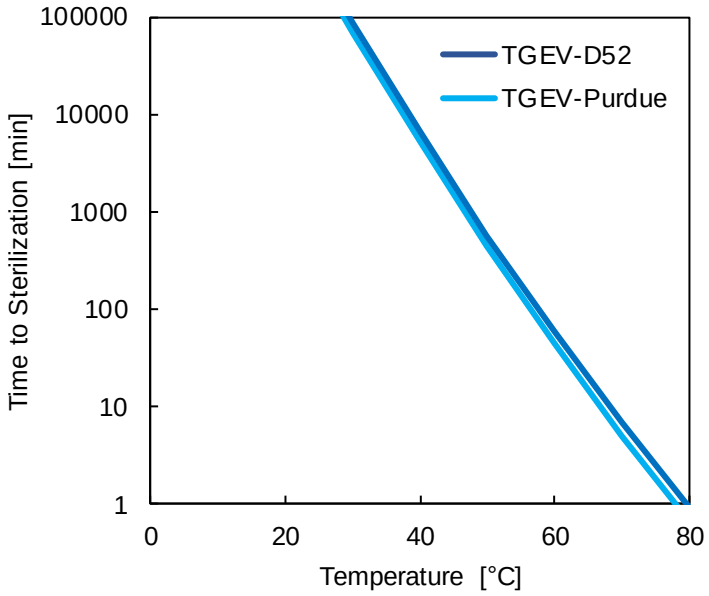

Figure S30. Model predictions for sterilization times required for the TGEV D52 and Purdue strains.

Trends across relative humidity conditions

Comparing results for the TGEV and MHV viruses at relative humidity levels of 20%, 50%, and 80%, we did not observe any clear trends, as shown in **Figures S31** and **S32**. We note that the dataset obtained from Casanova, et al., appeared to exhibit the most experimental error of all the data used in the model, especially at low temperatures, with R^2 values as low as 0.1 when applying linear fits to several sets of their data in **Section S1**. Therefore, more data would be needed to rule out a correlation between virus inactivation and relative humidity, especially considering such a trend has been implied in prior work.[44]

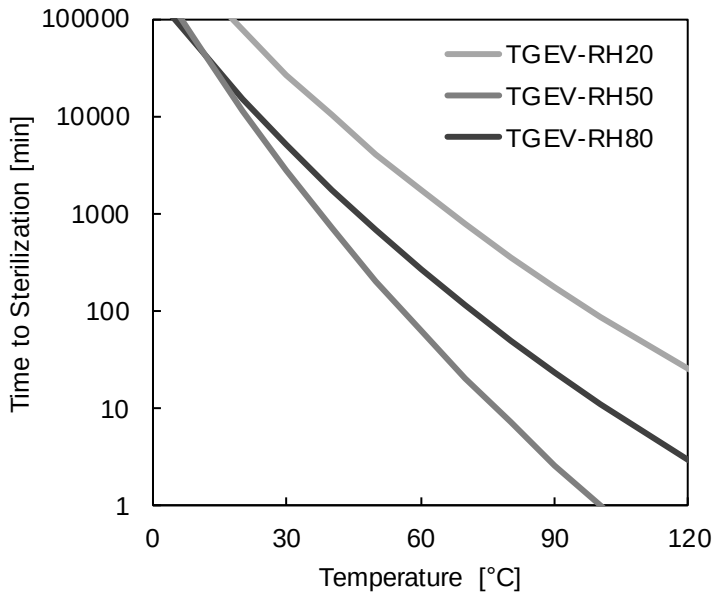

278

279 **Figure S31.** Model predictions for sterilization times required for TGEV at levels of relative humidity of

280 20%, 50%, and 80%.

281

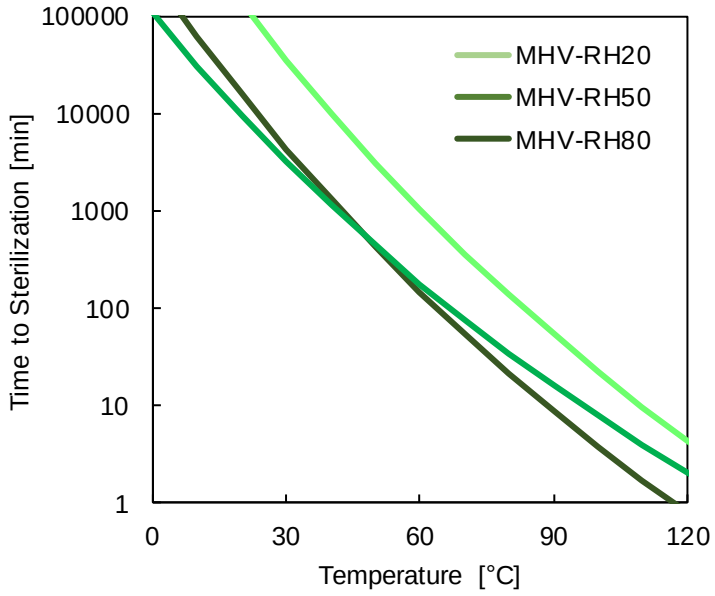

282

283 **Figure S32.** Model predictions for sterilization times required for MHV at levels of relative humidity of

284 20%, 50%, and 80%.

285

Trends across pH levels

Comparing results for PEDV across pH levels of 7.2, 9.2, and 10.2, we observed a faster rate of virus inactivation at more basic pH levels as reported in prior work,[29] shown here in **Figure S33**.

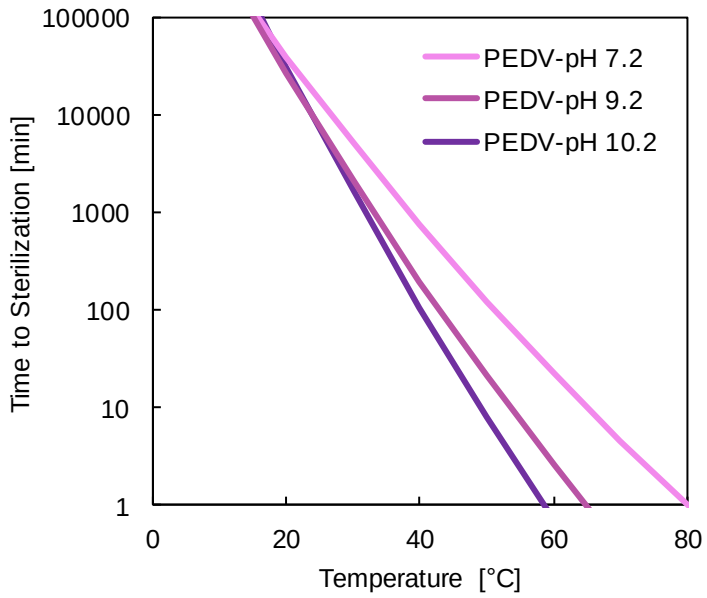

Figure S33. Model predictions for sterilization times required for PEDV at pH levels of 7.2, 9.2, and 10.2.

S4. Conversion of Climate Data to Inactivation Timescale Map

National average temperature maps of the United States for the months of January to March, 2020, and July to September, 2019, were obtained from the National Oceanic and Atmospheric Administration (NOAA). These temperature maps, shown in **Figures S34** and **S35**, display the CONUS mean temperature (except data for Hawaii and Alaska, which were obtained from NOAA's climate data online search). The average temperature values encompassing January through March, 2020, were chosen in accordance with the timeline of the COVID-19 pandemic to date, and the average temperature values from July to September, 2019, were chosen to represent typical summer weather in the United States.

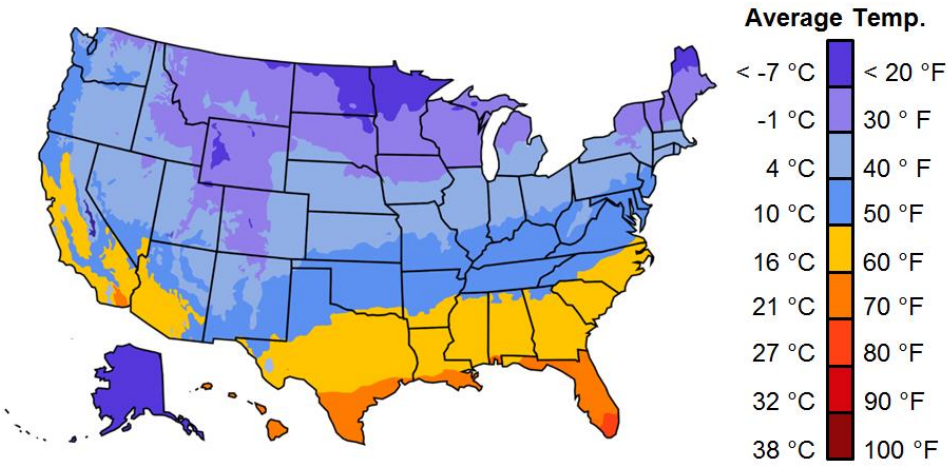

303

304 **Figure S34.** Initial data from NOAA used to generate **Figure 3** in the main text; average temperatures

305 over the period encompassing January to March, 2020, are shown.

306

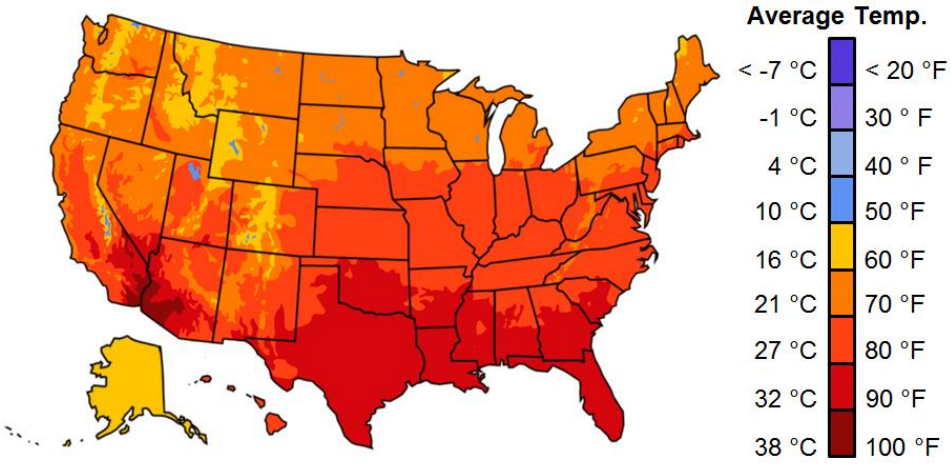

307

308 **Figure S35.** Initial data from NOAA used to generate **Figure 3** in the main text; average temperatures

309 over the period encompassing July to September, 2019, are shown.